THE ASTROPHYSICAL JOURNAL, 379:586–591, 1991 October 1

ECHO IMAGES OF BROAD-LINE REGIONS IN ACTIVE GALACTIC NUCLEI

WILLIAM F. WELSH
Astronomy Department, Ohio State University; and Space Telescope Science Institute, 3700 San Martin Drive, Baltimore, MD 21218
AND
KEITH HORNE
Space Telescope Science Institute, 3700 San Martin Drive, Baltimore, MD 21218
Received 1990 September 28; accepted 1991 April 18

ABSTRACT

Continuum and emission line variations can be used to form two-dimensional images of gas flows in the nuclear regions of active galaxies. The "echo image," $\Psi(v, \tau)$, is the two-dimensional transfer function that maps continuum variations to emission-line variations. Convolving a continuum light curve $C(t)$ with $\Psi(v, \tau)$ yields $L(v, t)$, the line light curve at each velocity across the line. A procedure for constructing the echo image of a given BLR model is described. Echo images for several BLR models are presented and discussed. A simulated continuum light curve is generated and convolved with the echo images to produce trailed spectrograms showing variations of the line fluxes and line profiles. Because the echo image incorporates both velocity and time-delay information, it is a far more powerful probe of the structure of the BLR than one-dimensional velocity profiles, transfer functions, or cross-correlation functions.

Subject headings: galaxies: nuclei — galaxies: Seyfert — line profiles — radiative transfer

1. INTRODUCTION

It is well established that some galaxies which possess an active nucleus exhibit nonperiodic variations in both their continuum and broad emission lines. Because of its proximity to the central engine, the broad-line emitting region (BLR) is expected to be a potent diagnostic of the mechanism powering the nucleus. For an overview of emission-line variability in the BLR, see Peterson (1988) and references therein.

The variations of the broad emission lines occur on remarkably short time scales, constraining the size of the BLR via light-crossing time (causality) arguments. The shapes of the continuum and line light curves are similar, with the line variations tending to be delayed with respect to the continuum variations. The time delay or lag, τ, defined as the difference between the observed arrival times of a continuum pulse and the associated line pulse, can be quantified by cross-correlating the two light curves. Noisy and unevenly sampled light curves complicate the calculation of the cross-correlation, but several different techniques have been developed (Gaskell & Sparke 1986; Gaskell & Peterson 1987; Edelson & Krolik 1988; Scargle 1989). The peak or centroid of the cross-correlation can provide a rough estimate for the characteristic or luminosity-weighted size of the BLR (for recent examples see Clavel et al. 1991; Peterson et al. 1991; Maoz et al. 1990, 1991; Koratkar & Gaskell 1991b). However, the lag must be interpreted with caution because it depends not only on the physical structure of the BLR but also on properties of the continuum variations. For further discussion and application of the cross-correlation technique to constrain BLR sizes, as well as kinematics; see, for example, Koratkar & Gaskell (1991a).

Using individual or time-averaged emission-line profiles in an attempt to unambiguously determine the motion of the emitting gas has proven to be a difficult task (Blumenthal & Mathews 1975; Capriotti, Foltz, & Byard 1980; but see Penston et al. 1990). Capriotti, Foltz, & Peterson (1982) and Blandford & McKee (1982) emphasized the importance of using the information contained in the time-varying line profiles. In particular, Blandford & McKee (1982) introduced the idea that the line profile variations, $L(v, t)$, are the result of the convolution of the continuum variations, $C(t)$, with a "transfer function", $\Psi(v, \tau)$,

$$L(v, t) = \int_0^\infty \Psi(v, \tau) C(t - \tau) d\tau ,$$

where v denotes velocity and t denotes time. We regard $\Psi(v, \tau)$ as a two-dimensional map, which we shall refer to as the "echo image" of the BLR. The echo image is a projection of the BLR's six-dimensional phase-space distribution (although see Penston 1990 for possible limitations of this view).

Determining $\Psi(v, \tau)$ from noisy and irregularly sampled light curves is a difficult deconvolution problem. Blandford & McKee (1982) showed that Fourier inversion methods can be used to get $\Psi(v,\tau)$, but the limited quality data then available delayed further development of this idea.

Recent data of much higher quality has been obtained through the organization of the Herculean monitoring campaigns (e.g., Maoz et al. 1990; Clavel et al. 1991; Peterson et al. 1991). This is sparking renewed interest in modeling transfer functions (e.g., Robinson & Perez 1990), and in improved deconvolution methods (such as the maximum entropy method) to invert the data to find the one-dimensional "echo function" $\Psi(\tau)$ (Horne, Welsh, & Peterson 1991; Maoz et al. 1991; Krolik et al. 1991). The full two-dimensional echo image $\Psi(v, \tau)$ can be recovered by dividing the line profiles into velocity bins and applying the one-dimensional mapping technique to the line light curves obtained from each velocity bin. Results of the two-dimensional "echo mapping" inversion will be reported in forthcoming papers.

Because the appearance of the two-dimensional echo image for a given BLR model is not immediately obvious, we have constructed and present here echo images from several simple, but representative models. By considering these cases, the reader may develop an understanding of the sense in which

$\Psi(v, \tau)$ represents a two-dimensional map of the BLR. We stress that these models are chosen mainly for pedagogical purposes, not because we feel they are accurate representations of the BLR (evidence exists for the exclusion of some of these models;—see for example Gaskell 1988; Koratkar & Gaskell 1989; Crenshaw & Blackwell 1990; Koratkar & Gaskell 1991a, b; Stirpe & de Bruyn 1991). In § 2 we give a prescription for constructing echo images for spherical inflow, outflow, and disk BLR models. Section 3 describes the BLR models that have been employed, and § 4 presents the echo images produced. In § 5 we present the results of convolving the echo images with a simulated continuum light curve, producing trailed spectrograms that display the line profile variations.

2. CONSTRUCTION OF AN ECHO IMAGE FROM A BLR MODEL

Figure 1 illustrates the construction of echo images for three specific BLR models: a constant velocity $V(r) = 10{,}000$ km s^{-1} spherical outflow (Fig. 1*a*), spherical free-fall into a $10^8\ M_\odot$ point-mass potential (Fig. 1*b*), and a thin Keplerian disk around a $10^8\ M_\odot$ central object Fig. (1*c*). In all three cases the solid line represents the contribution to the echo image that originates from the innermost radius ($r_{\rm min} = 5$ light days), the dashed line represents the contribution from material at the outermost radius ($r_{\rm max} = 50$ light days), and the dotted lines correspond to material located at intermediate radii.

In spherically symmetric geometries, each shell of radius r and outward velocity $V(r)$ maps onto a diagonal line in the velocity-delay (v, τ) plane. At an angle θ measured from the back point of the shell, furthest from the observer, the velocity component along our line of sight is

$$v = V(r) \cos\theta ,$$

and the time delay is given by

$$\tau = \frac{r}{c}(1 + \cos\theta) .$$

Combining these expressions we get

$$\tau(v, r) = \frac{r}{c}\left[1 + \frac{v}{V(r)}\right] .$$

Thus each spherical shell maps onto a diagonal line in the v-τ plane with $\cos\theta$ increasing uniformly along the diagonal line. The terminal points of this line ($\cos\theta = -1$ at the front and $\cos\theta = +1$ at the back of the shell) occur at $(\tau, v) = (-V(r), 0)$ and $(V(r), +2r/c)$. The slope of the line ($d\tau/dv = r/cV$), is positive for outflow and negative for inflow. The τ-intercept at r/c is independent of the velocity law. Note that inflow and outflow cases are mirror images of each other reflected about the τ-axis. Thus the echo image for spherical geometries will consist of the union of many diagonal lines, each line corresponding to a different shell. Note the caustic which appears in Figure 1*b*, a general feature of spherical geometries with velocity laws that increase inward.

For the Keplerian disk, the ellipses in Figure 1*c* correspond to rings of radius r, where the circular velocity is $V(r) = (GM/r)^{1/2}$. The observed velocity and time delay are

$$v = V(r) \sin i \sin\phi ,$$

$$\tau = \frac{r}{c}(1 - \sin i \cos\phi) ,$$

where i is the inclination of the axis of the disk to our line of sight ($0 \le i \le 90°$) and ϕ is the azimuthal angle between a point on the disk and the projection of the line of sight onto the disk. Combining these we get

$$\left[\frac{\tau - (r/c)}{r/c}\right]^2 + \left[\frac{v}{V(r)}\right]^2 = \sin^2 i$$

which is the equation for an ellipse centered at $(v, \tau) = (0, r/c)$ and spanning $\pm V \sin i$ in velocity and $(r/c) \sin i$ in time delay. For a fixed inclination, as r increases, the center of the associated ellipse moves up the τ-axis. For a fixed radius, as i decreases, the axes of the ellipse shrink to zero and the ellipse degenerates to a point.

3. POWER-LAW BLR MODELS

While the mapping from a BLR model to an echo image is straightforward, the choice of the BLR model is somewhat problematic because so little is certain about the dynamics and radiative transfer in the BLR. We allow the velocity field V, the number of clouds dN in a given radius interval, and the emissivity per cloud ϵ to be power-law functions of the distance from the center r:

$$V(r) = V_0(r/r_{\rm min})^\alpha , \quad dN(r) = N_0(r/r_{\rm min})^\beta\, dr ,$$

$$\epsilon(r) = \epsilon_0(r/r_{\rm min})^\gamma .$$

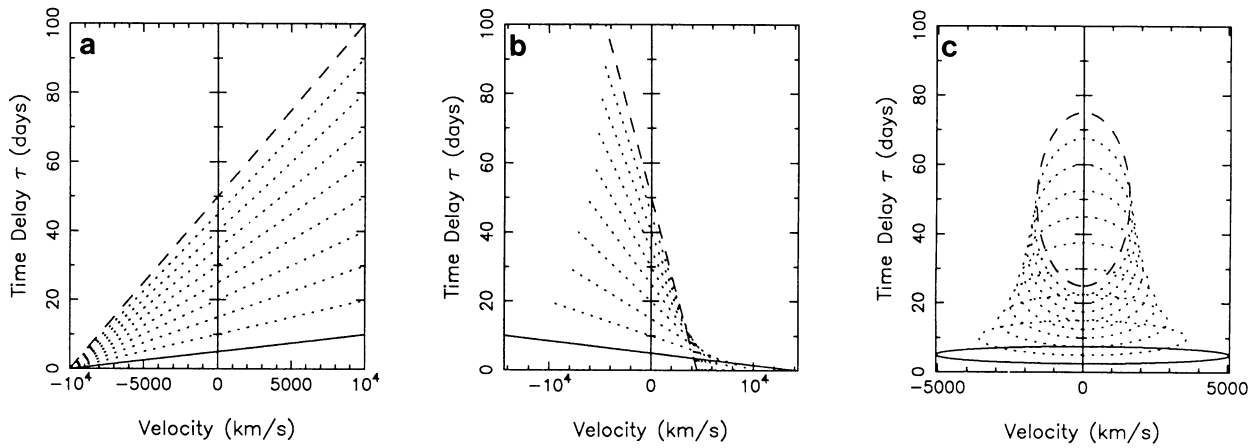

FIG. 1.—Sketches of the echo image for three different BLR models as described in the text. (*a*) Spherically symmetric constant velocity outflow. (*b*) Spherically symmetric free-fall inflow. (*c*) Thin Keplerian disk at an inclination of 30°.

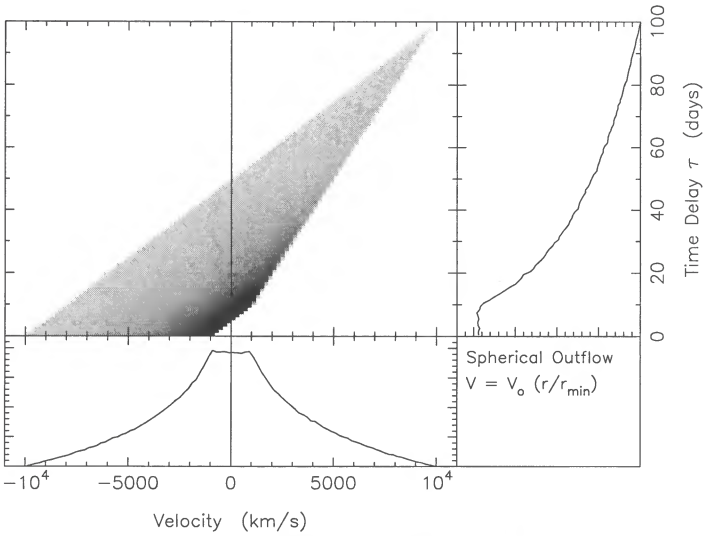

FIG. 2.—Echo image for a spherically symmetric outflow BLR model. The velocity law is a Hubble-type expansion with $V_0 = 1000$ km s^{-1}. The echo image is integrated over velocity to produce the one-dimensional echo function shown in the upper right. The lower left panel shows the line profile generated by integrating the echo image over time delay.

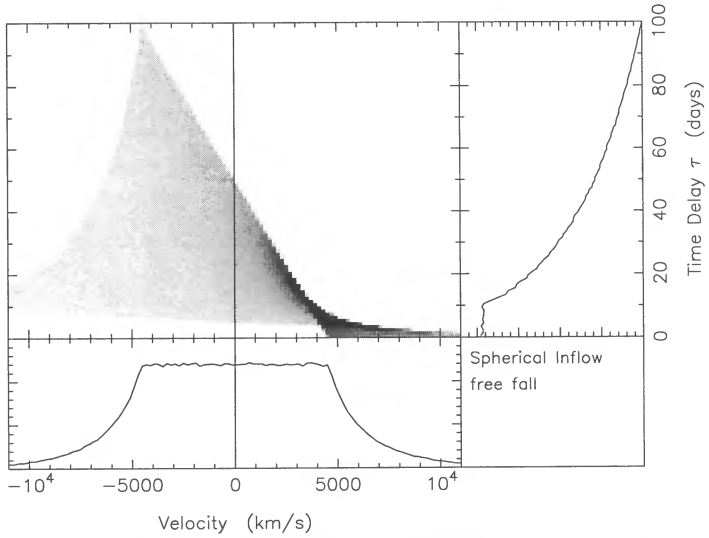

FIG. 3.—Echo image for a spherically symmetric free-fall inflow BLR model. Note the similarity between this one-dimensional echo function and that of Fig. 2.

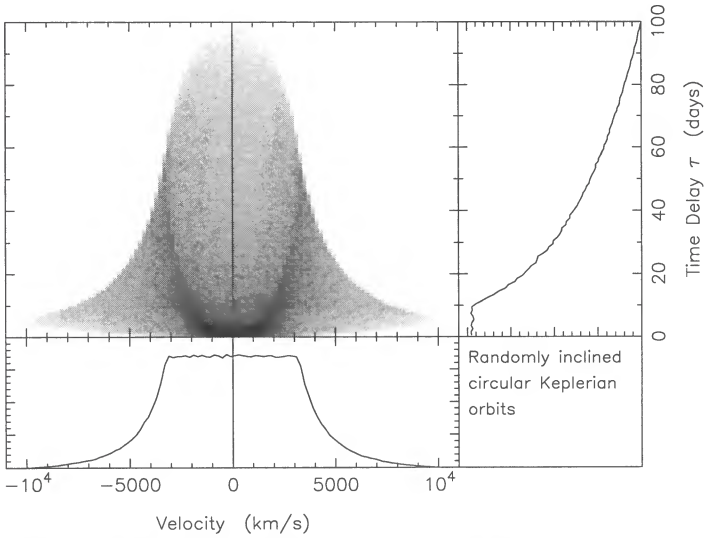

FIG. 4.—Echo image for a spherically symmetric BLR model consisting of clouds on randomly oriented circular orbits. Note the similarity between this one-dimensional echo function and those of Figs. 2 and 3.

Other parameters which must be specified include the geometry, r_{min} and r_{max}, and the mass of the central object (if V_0 is not to be arbitrarily chosen). We consider only spherical and thin disk geometries, and since the numerical value of the central mass only rescales the problem, it can be fixed at 10^8 $M_\odot$ with no loss of generality. The model is constructed by generating many random cloud positions distributed throughout the sphere or disk. In practice, the radial coordinate is broken up into equal segments, and each segment is assigned its own value of $dN(r)$. Each point in the model BLR's, six-dimensional phase space maps directly to a point in the observed velocity-time delay plane with a weight determined by the cloud emissivity. Many different BLR structures can be easily accomodated within this framework. In this paper we consider a few selected models so that the reader may gain an intuitive feeling for the echo image. More elaborate models such as a combination of a disk with a wind may be easily constructed. Implicit in our current models are the following assumptions/limitations: (1) all photons are radiated isotropically, (2) there is no obscuration by intervening clouds or dust, (3) the clouds are identical, discrete emitters, (4) the emission lines respond linearly and instantaneously to the continuum variations, (5) the echo functions are time independent (the BLR structure is constant), (6) the ionizing continuum originates from a pointlike source located at the center, (7) relativistic effects have been ignored. These assumptions can be lifted in a straightforward but model-dependent manner.

4. ILLUSTRATIVE EXAMPLES OF ECHO IMAGES

In the examples that follow, we use an inner radius r_{min} of 5 light-days and an outer radius r_{max} of 50 light days. These were chosen primarily for illustrative purposes, although r_{max} was chosen with the knowledge that the echo functions determined for NGC 5548 (Horne et al. 1991) and NGC 4151 (Maoz et al. 1991) do not seem to show much power beyond 50 days or so [also, the ratio $(r_{max}/r_{min}) \sim 10$ may be a general property of all BLRs. See Koratkar & Gaskell 1991b]. We constructed each of the echo images using velocity pixels of 200 km/s, τ pixels of 1 day, and radial zones set at a width of a tenth of a light-day. In all cases, $\sim 760{,}000$ points were used to "pepper" the image.

Figures 2–5 display a series of echo images. These figures show a gray-scale representation of the echo image $\Psi(v, \tau)$. This is integrated over velocity to produce the one-dimensional echo function $\Psi(\tau)$ (*upper right*) and integrated over time delay to produce a velocity profile $\Psi(v)$ (*lower left*). The line profile generated can be compared with the observable variability spectrum, and the echo function can be compared with echo function derived from the observed continuum and line light curves. Be aware, however, that the velocity profile here is that of the variations in the line, and is insensitive to any constant components.

In Figure 2 we consider the echo image of a spherical outflow model. The velocity law was chosen to be linear in r ($\alpha = 1.0$) which is a Hubble-type flow. For simplicity we choose

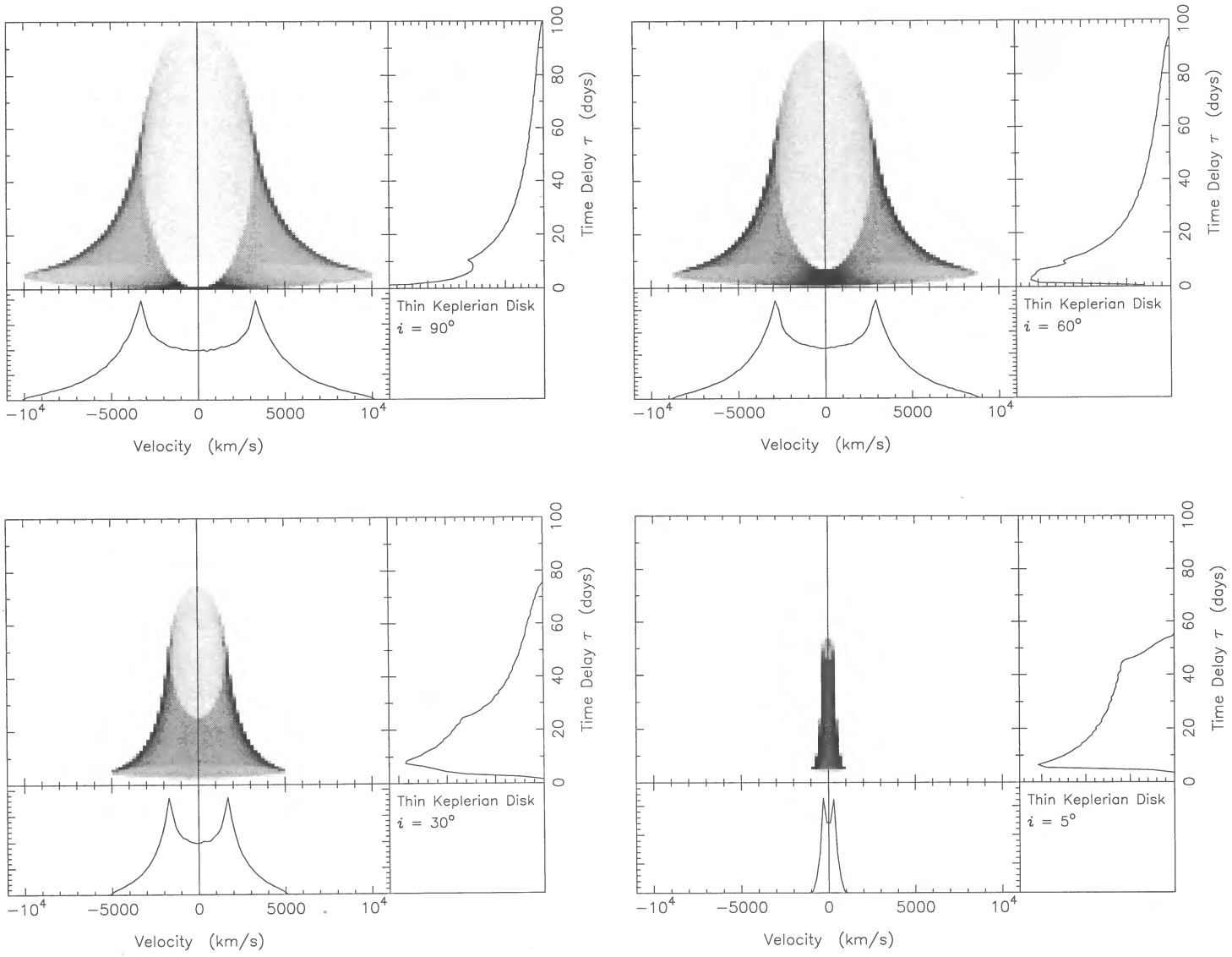

FIG. 5c FIG. 5d

FIG. 5.—Echo image for a thin Keplerian disk BLR model viewed at an inclination of (*a*) 90° (edge on), (*b*) 60°, (*c*) 30°, (*d*) 5°.

$\gamma = 0$ so that each cloud is equally bright, and $\beta = 0$ so that $dN(r) =$ constant. The choice of V_0 was arbitrary. As in Figures 1*a* and 1*b*, spherical BLRs map into a series of diagonal lines, and for our power-law velocity laws the slopes of the lines are $d\tau/dv = \pm(r_{\rm min}^{\alpha}/cV_0)r^{(1-\alpha)}$. Since $\alpha = 1$ here, the slopes are constant. The one-dimensional echo function $\Psi(\tau)$ has a flat top out to $2r_{\rm min} = 10$ days and then declines smoothly to zero at $2r_{\rm max} = 100$ days. The velocity profile has a flat top between $\pm V(r_{\rm min})$ and wings extending to $\pm V(r_{\rm max})$.

Figure 3 shows a spherical inflow model assuming a free-fall velocity law, $V(r) = -(2GM/r)^{1/2}$ (compare with the schematic shown in Fig. 1*b*). Values of β and γ were chosen to be equal to zero for simplicity. Note that time delays are much smaller on the red side of the line, a general characteristic of infalling BLRs.

Figure 4 shows the echo image of a spherical BLR consisting of clouds on randomly oriented circular Keplerian orbits. The projected velocity and time delay expressions are the same as in the disk case, except that the inclination is now in random directions. Alternately, one can use the time delay expression for radial motion in a spherical geometry and $v = -V(r)\sin\theta$, provided that $V(r)$ is now considered to be pointing in a random direction tangent to the surface of the sphere. Again β and γ were set to zero, to allow direct comparison with Figures 2 and 3. Note that the models in Figures 2, 3, and 4 have identical echo functions, yet are easily distinguishable when viewed as a two-dimensional echo image.

Figures 5*a*–5*d* show the echo image of a thin Keplerian disk viewed at different inclinations (compare with Fig. 1*c*). In these models we chose $\gamma = 0$ as before, but now set $\beta = -0.5$. This has the effect of simulating a surface brightness that goes as $r^{-3/2}$, similar to the observed behavior of the surface brightness distribution in the accretion disks of cataclysmic variables (e.g., Marsh et al. 1990). The ellipses centered at $\tau = 5$ days and 50 days, corresponding to the inner and outer radii, are clearly visible. At an inclination of 90° (Fig. 5*a*), every ellipse touches the $(v, \tau) = (0, 0)$ point, thus the projection $\Psi(\tau)$ has a sharp peak at $\tau = 0$. Notice how the inner and outer ellipses generate

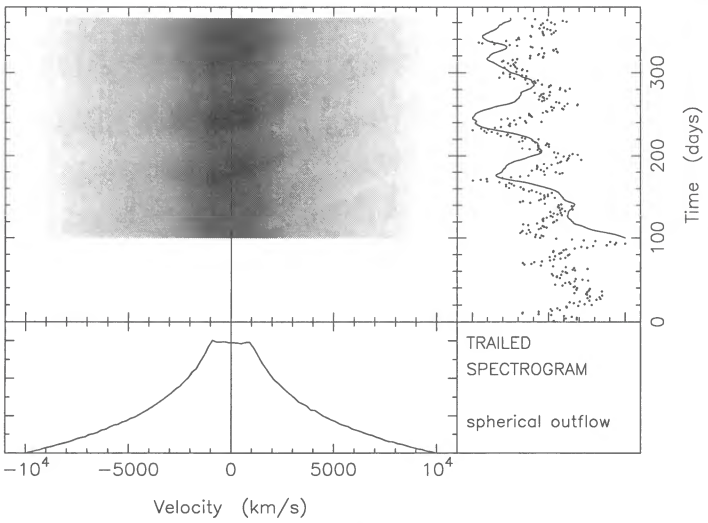

FIG. 6.—Panel 1 shows a trailed spectrogram constructed by convolving the echo image from the spherical Hubble-type outflow BLR model (see Fig. 2) with a simulated continuum light curve (shown as dotted line in upper right panel). The trailed spectrogram for times prior to day 100 are not shown because the convolution is not defined there. Also shown in the upper right is the total line flux light curve (*solid line*). The time-averaged line profile is shown in the lower left panel.

kinks in $\Psi(\tau)$, and how the double-peaked velocity profile is produced by the velocity of the outer ring. As the inclination is decreased (Fig. 5*b*–5*d*) each ellipse remains centered at $(v, \tau) = (0, r/c)$ but shrinks in proportion to sin i. In the limit of a face-on disk, the ellipses shrink to points on the $v = 0$ axis, and the resulting one-dimensional echo function directly gives the radial emissivity profile of the disk.

5. SIMULATED TRAILED SPECTROGRAMS

The echo image is simply the echo function at each velocity across the line. The line light curve at a given velocity is then the convolution of the continuum light curve with the appropriate slice of the echo image. The line light curves can be displayed alongside each other to form a "trailed spectrogram," a two-dimenional light curve whose axes are velocity and time.

The trailed spectrograms shown in Figures 6–8 were produced by convolving the same simulated continuum light curve with different echo images. We modeled the continuum light curve as a random walk in flux, $C(t + \Delta t) = C(t) + R$, where R is a random number uniformly distributed over the interval $(-1, 1)$, i.e., $C(T)$ is a realization of a one-sided autoregressive process of order 1; see Scargle 1981 and references therein. The power spectrum of this type of light curve is a power law in frequency with a slope of -2, similar to that observed in NGC 5548 (Krolik et al. 1991). The echo images used are those previously discussed: spherical outflow (Fig. 2), inflow (Fig. 3), and a Keplerian disk at $i = 60°$ (Fig. 5*b*). One can see the "ghosts" of the echo image in the trailed spectrograms. It is important to keep in mind that these trailed spectrograms lie in the observable velocity and time space and can be directly compared to data. The simulated continuum light curve is shown in the upper right corner (*dotted line*) along with the light curve of the total flux in the emission line (*solid line*). These two curves were normalized by subtracting off their minimum value, then dividing by their peak-to-peak difference.

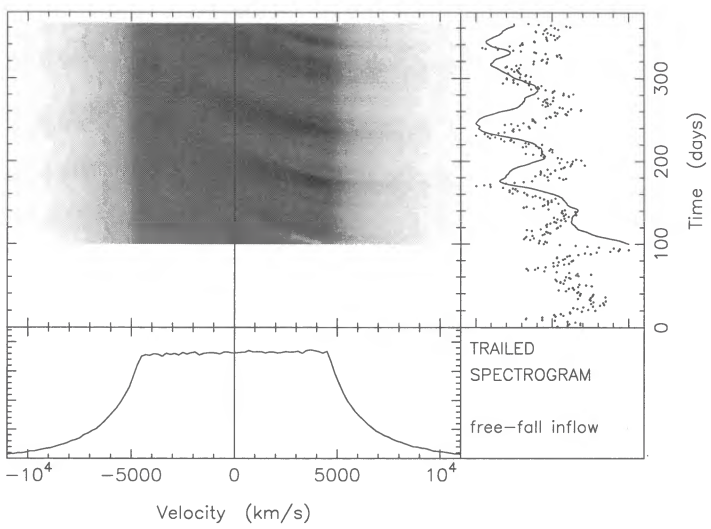

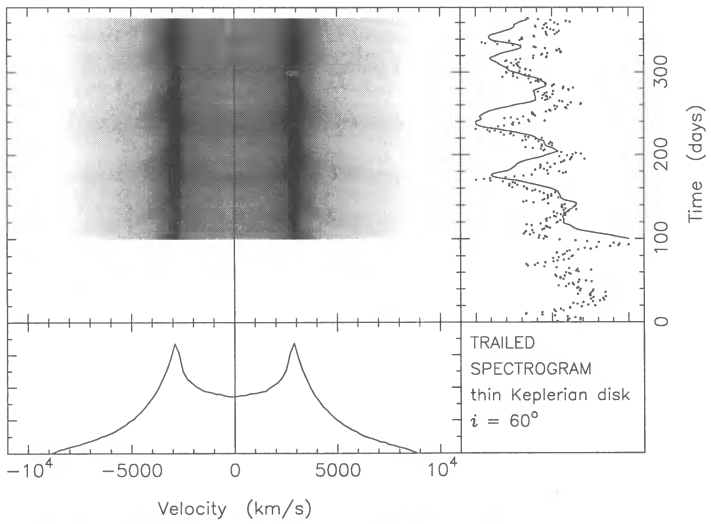

FIG. 8.—Trailed spectrogram for a thin Keplerian disk at an inclination of 60° (see Fig. 5*b*).

Notice that the emission line light curves in the two spherical cases are very similar; they would be indistinguishable if noise were introduced. This reemphasizes the point that using only the total line flux instead of the flux at each velocity can lead to ambiguous interpretation of the BLR structure. The line profile, integrated over the duration of the light curve is shown in the lower left panel.

If the continuum light curve were a delta function pulse, the echo image would clearly be visible in the trailed spectrogram because one pulse in the continuum produces one manifestation of the echo image. Even when the continuum is constantly changing, the varying continuum can be thought of as a series of delta functions of different amplitudes packed one immediately after the other. So the trailed spectrogram is likewise a series of echo images of different amplitudes packed one immediately after the start of the other. The effect is to produce overlapping echo images in time, as seen in Figures 6–8.

6. CONCLUSIONS

We have developed the concept and appearance of a two-dimensional "echo image," $\Psi(v, \tau)$, a transfer function that maps continuum variations to emission-line variations at each velocity across the line. Because the one-dimensional echo function is determined solely by variations as a function of time, it is sensitive only to radial distance, or more correctly, to the geometry of the BLR. The two-dimensional echo image includes line profile information and is sensitive to both the geometry and the velocity field; thus it is a better discriminator of BLR models than the one-dimensional echo function or cross correlation. We demonstrated cases with identical one-dimensional echo functions which were easily distinguished by their two-dimensional echo images.

We describe a procedure for constructing an echo image $\Psi(v, \tau)$ from a given BLR model and present the echo images of a selection of power-law BLR models. We consider spherical accelerated outflow, spherical free-fall inflow, a thin Keplerian disk at various inclinations, and circular Keplerian orbits at random orientations. We show how such ordered velocity fields allow us to consider the echo image as a two-dimensional map of the BLR, separating out the emission at different radii and azimuths. By convolving a simulated continuum with the echo images, line profile variations are computed and the results presented in the form of trailed spectrograms. In forthcoming papers we consider the inverse problem, solving for the two-dimensional echo image from the observed continuum and line profile variations.

We thank Brad Peterson and Anuradha Koratkar for advice and helpful comments. W. F. W. is grateful to the STScI Graduate Student Program and to the National Aeronautics and Space Administration and the National Science Foundation through grants NAG5-1366 and AST 89-15258, respectively, to the Ohio State University for support of this work. This research was partially supported by NASA grant NAGW-1796.

REFERENCES

Blandford, R. D., & McKee, C. F. 1982, ApJ, 255, 419
Blumenthal, G. R., & Mathews, W. G. 1975, AJ, 198, 517
Capriotti, E. R., Foltz, C. B., & Byard, P. L. 1980, ApJ, 241, 903
Capriotti, E. R., Foltz, C. B., & Peterson, B. M. 1982, ApJ, 251, 35
Clavel, J., et al. 1991, ApJ, 366, 64
Crenshaw, D. M., & Blackwell, J. H. Jr. 1990, ApJ, 358, L37
Edelson, R. A., & Krolik, J. H. 1988, ApJ, 333, 646
Gaskell, C. M. 1988, ApJ, 325, 114
Gaskell, C. M., & Peterson, B. M. 1987, ApJS, 65, 1
Gaskell, C. M., & Sparke, L. S. 1986, ApJ, 305, 175
Horne, K., Welsh, W. F., & Peterson, B. M. 1991, ApJ, 367, L5
Koratkar, A. P., & Gaskell, C. M. 1989, ApJ, 345, 637
———. 1991a, ApJ, 375, 85
———. 1991b, ApJS, 75, 719
Krolik, J. H., Horne, K., Kallman, T. R., Malkan, M. A., Edelson, R. A., & Kriss, G. A. 1991, ApJ, 371, 541
Maoz, D., Netzer, H., Leibowitz, E., Brosch, N., Laor, A., Mendelson, H., Beck, S., Almoznino, E., & Mazeh, T. 1990, ApJ, 351, 75
Maoz, D., Netzer, H., Mazeh, T., Beck, S., Almoznino, E., Leibowitz, E., Brosch, N., Mendelson, H., Laor, A. 1991, ApJ, 367, 493
Marsh, T. M., Horne, K., Schlegel, E. M., Honeycutt, R. K., & Kaitchuck, R. H. 1990, ApJ, 364, 637
Penston, M. V. 1990, QJRAS, submitted
Penston, M. V., Croft, S., Basu, D., & Fuller, N. 1990, MNRAS, 244, 357
Peterson, B. M. 1988, PASP, 100, 18
Peterson, B. M., et al. 1991, ApJ, 368, 119
Robinson, A., & Perez, E. 1990, MNRAS, 244, 138
Scargle, J. D. 1981, ApJS, 45, 1
———. 1989, ApJ, 343, 874
Stirpe, G. M., & de Bruyn, A. G. 1991, A&A, in press

Note added in proof.—It has come to the attention of the authors that Pérez, Robinson, & de la Fuente are also investigating the appearance of the two-dimensional transfer functions of the BLR. An atlas is being constructed which covers a wider range of parameters and includes a biconical geometry model.